Relaxation of a supercooled low-density Coulomb fluid

S. D. Wilke and J. Bosse*
Freie Universität Berlin, Institut für Theoretische Physik, Arnimallee 14, D-14195 Berlin, Germany
(Received 6 July 1998)

A system of charged hard spheres in front of a homogeneous neutralizing background is studied at low densities using mode-coupling theory. A ''Wigner glass'' phase, the amorphous analog of the Wigner crystal recently found in experiments, is predicted. The melting curve of the Wigner glass obeys $n \propto T^3$, and the particle localization length is much larger than the Lindemann criterion would predict. An analysis of transport properties shows that huge effective particle diameters are responsible for the glassification at low densities. The Stokes-Einstein relation, which is obeyed by the high-density fluid, implies large Stokes radii at low densities. [S1063-651X(99)02702-6]

PACS number(s): 64.70.Pf, 66.10.−x, 66.20.+d

I. INTRODUCTION

The density at which solids can be formed from individual particles is limited by the range of their interaction potential. Short-range forces can only bind particles at high densities, while long-range forces, e.g., the Coulomb interaction, are capable of forming solids even at very low densities. Back in 1938, Wigner predicted the existence of such a low-density Coulomb solid for electron systems, the so-called Wigner crystal [1]. Recently, the first, to our knowledge, experimental realizations of Wigner crystals have been found, not only in electron systems [2] but, for example, with charged colloidal particles in aqueous solution [3] and charged dust particles in plasmas [4,5].

However, it may be possible that low-density solids do not always have a crystalline structure. As already pointed out by Aoki [6], there may also be *amorphous* low-density solids, for which the term ''Wigner glass'' seems appropriate. Figure 2 of Ref. [5], for example, shows a structure that could be interpreted as somewhere in between crystalline and amorphous phase. Experimentally, the Wigner glass phase could be reached—in analogy to the well-known high-density glass phase—by supercooling (or supercompressing) a low-density Coulomb fluid. Because of this analogy, it seems reasonable to attempt a theoretical description of the Wigner glass using the same concepts that are employed for the glass transition at *high* densities, for example the mode-coupling theory (MCT) [7,8], which has been very successful in describing the glass transition of fragile glass-forming liquids.

It was shown in a previous publication [9] that MCT indeed predicts a low-density glass phase for the so-called restricted primitive model (RPM), a two-component symmetrical charged hard-sphere system. Further studies have then revealed that the ability of forming a Wigner glass from a binary fluid of charged particles depends neither on charge ratio, nor on diameter ratio or mass ratio [10]. The MCT phase diagrams of binary and one-component charged hard-sphere systems *all* show a low-density glass phase. This result supports the view that it is the long-ranged Coulomb interaction potential that is mainly responsible for the formation of a Wigner solid.

In this paper, we will give a detailed account of the results of MCT for one specific model system which seems suitable for comparison with experiments: a fluid of charged hard spheres in front of a homogeneous neutralizing background. This model system, which we will refer to as hard-sphere jellium (HSJ), is very similar to the well-known one-component plasma (OCP), and could be used to describe dusty plasmas and colloidal systems in which Wigner crystals have been observed.

The paper is organized as follows: Following this introduction, we present a summary of MCT for the HSJ in Sec. II. Our results include a fluid-glass phase diagram (Sec. III), Debye-Waller factors (Sec. IV), relaxation behavior (Sec. V), and transport properties (Sec. VI) of the HSJ. A critical review of the obtained results is given in the conclusion in Sec. VII.

II. FORMAL FRAMEWORK

Starting point of the theoretical analysis of the HSJ is a classical, homogeneous, isotropic *two*-component fluid of oppositely charged particles, the second species of which is to become the homogeneous background. The MCT for such a two-component fluid is formulated in terms of the Kubo relaxation functions

$$\hat{\Phi}_{ss'}(q;t) := \beta \langle \delta N^{(s)}(\mathbf{q},t)^{\dagger} \delta N^{(s')}(\mathbf{q}) \rangle \tag{1}$$

of the partial number density fluctuations $\delta N^{(s)}(\mathbf{q}) := N^{(s)}(\mathbf{q}) - \langle N^{(s)}(\mathbf{q}) \rangle$ with $N^{(s)}(\mathbf{q}) := \sum_{j=1}^{N_s} \exp[-i\mathbf{q}\cdot\mathbf{r}_j^{(s)}]/\sqrt{N_s}$, where $s=1,2$ is the species index, N_s the number of particles of species s, $\beta := 1/(k_B T)$, and $\langle \cdots \rangle$ denotes a thermal equilibrium average. The thermodynamic limit is to be taken at the end of the calculations. With the help of the Mori-Zwanzig projection-operator method [11,12] a formally exact equation of motion is derived for the matrix of relaxation functions $\hat{\Phi}(q;t)$ resulting in

$$\hat{\Phi}(q,z) = -\{z - [z + \hat{K}(q,z)]^{-1} \cdot \hat{\Omega}^2(q)\}^{-1} \cdot \hat{\Phi}(q;t=0) \tag{2}$$

*Author to whom correspondence should be addressed.

for the matrix of Fourier-Laplace transforms $\hat{\Phi}(q,z) := i\int_0^\infty dt \exp(itz)\hat{\Phi}(q;t)$. The initial condition for the relaxation function is given by the matrix $\hat{S}(q)$ of the partial static structure factors, i.e., $\hat{\Phi}(q;t=0)=\beta\hat{S}(q)$. The frequency matrix $\hat{\Omega}^2(q)$ can also be expressed in terms of the static structure,

$$\hat{\Omega}^2_{ss'}(q) := \frac{q^2}{\beta m_s}[\hat{S}^{-1}(q)]_{ss'}, \tag{3}$$

where m_s is the particle mass of species s. Within MCT, the matrix of relaxation kernels $\hat{K}(q,z)$ is approximated as the sum

$$\hat{K}(q,z)=\hat{K}^{\mathrm{reg}}(q,z)+\hat{K}^{\mathrm{MC}}(q,z) \tag{4}$$

of a regular contribution $\hat{K}^{\mathrm{reg}}(q,z)$, with $z\hat{K}^{\mathrm{reg}}_{ss'}(q,z)\to 0$ for small z, and a mode-coupling part describing the nonlinear feedback of density fluctuations on the relaxation,

$$\hat{K}^{\mathrm{MC}}(q;t)_{ss'}=\sum_{\mathbf{k},\mathbf{p}}\sum_{\sigma,\sigma'=1}^{2}\sum_{\mu,\mu'=1}^{2}\hat{V}(ss'\mathbf{q};\sigma\sigma'\mathbf{k};\mu\mu'\mathbf{p}) \times\hat{\Phi}_{\mu\mu'}(p;t)\hat{\Phi}_{\sigma\sigma'}(k;t), \tag{5}$$

$$\hat{V}(ss'\mathbf{q};\sigma\sigma'\mathbf{k};\mu\mu'\mathbf{p}) := \frac{1}{V}\frac{\delta_{\mathbf{p},\mathbf{q}-\mathbf{k}}}{2\beta^3 m_s}[k_\parallel\delta_{s\mu}\sqrt{n_\sigma}\hat{c}_{\sigma\mu}(k)+p_\parallel\delta_{s\sigma}\sqrt{n_\mu}\hat{c}_{\mu\sigma}(p)] \times[k_\parallel\delta_{s'\mu'}\sqrt{n_{\sigma'}}\hat{c}_{\sigma'\mu'}(k)+p_\parallel\delta_{s'\sigma'}\sqrt{n_{\mu'}}\hat{c}_{\mu'\sigma'}(p)]. \tag{6}$$

The function $\hat{c}_{ss'}(q)$ is the Ornstein-Zernike direct correlation function, $n_s := N_s/V$ denotes the partial mean number density of species s, while $k_\parallel := \mathbf{k}\cdot\mathbf{q}/q$ and $p_\parallel := \mathbf{p}\cdot\mathbf{q}/q$. The mode-coupling contribution to the memory kernel will be responsible for the extremely slow relaxation of density fluctuations near the glass transition. A more detailed description of the mode-coupling approximation for multicomponent systems can be found in Ref. [13]. Since $\hat{K}^{\mathrm{MC}}(q;t)$ is expressed in terms of the relaxation function itself, Eq. (2) becomes a closed nonlinear integro-differential equation to be solved numerically for $\hat{\Phi}(q;t)$. The only input information required are the static structure factors $\hat{S}_{ss'}(q)$.

To introduce a neutralizing background to the two-component system described by Eqs. (2), (5), and (6), species 2 is ''smeared out'' across the system by setting $\hat{g}_{12}(r)\equiv 1$ and $\hat{g}_{22}(r)\equiv 1$ for the corresponding matrix elements of the radial distribution function. This results in a greatly simplified static structure,

$$\hat{S}(q)=\begin{pmatrix} S(q) & 0 \\ 0 & 1 \end{pmatrix}, \quad \hat{c}(q)=\begin{pmatrix} c(q) & 0 \\ 0 & 0 \end{pmatrix}, \tag{7}$$

where $S(q) := \hat{S}_{11}(q)$ and $c(q) := \hat{c}_{11}(q) = [1 - S_{11}(q)^{-1}]/n_1$. The frequency matrix, Eq. (3), takes on the form

$$\hat{\Omega}^2(q)=\begin{pmatrix} \Omega^2(q) & 0 \\ 0 & 0 \end{pmatrix}, \quad \Omega^2(q) := \frac{q^2}{\beta m_1 S(q)}. \tag{8}$$

The vertex function $\hat{V}(ss'\mathbf{q};\sigma\sigma'\mathbf{k};\mu\mu'\mathbf{p})$ from Eq. (6) vanishes unless $s=s'=\sigma=\sigma'=\mu=\mu'=1$. Therefore, only the (1,1) elements of $\hat{\Phi}(q;t)$ and $\hat{K}^{\mathrm{MC}}(q;t)$ are nonzero,

$$\hat{\Phi}(q;t)=:\begin{pmatrix} \Phi(q;t) & 0 \\ 0 & 0 \end{pmatrix}, \quad \hat{K}^{\mathrm{MC}}(q;t)=:\begin{pmatrix} K^{\mathrm{MC}}(q;t) & 0 \\ 0 & 0 \end{pmatrix}. \tag{9}$$

This means that the background does not show mode-coupling effects and thus no slowing down of relaxation processes when approaching the glass transition. The equation of motion, Eq. (2), decouples into two scalar equations if the regular part of the memory kernel can be neglected. This will be the case for times beyond the microscopic time scale near the glass transition, resulting in a complete decoupling of the particle motion from the background dynamics. The explicit form of the mode-coupling relaxation kernel, Eqs. (5) and (6), reduces to

$$K^{\mathrm{MC}}(q;t)=\sum_{\mathbf{kp}} V(\mathbf{q};\mathbf{k};\mathbf{p})\Phi(k;t)\Phi(p;t), \tag{10}$$

$$V(\mathbf{q};\mathbf{k};\mathbf{p}) := \hat{V}(1,1,\mathbf{q};1,1,\mathbf{k};1,1,\mathbf{p}) = \frac{n_1}{\beta^3 m_1}\frac{1}{V}\delta_{\mathbf{p},\mathbf{q}-\mathbf{k}}[k_\parallel c(k)+p_\parallel c(p)]^2. \tag{11}$$

Since, in the HSJ considered here, the background should not contribute to the packing fraction $\eta := \pi n\sigma^3/6$ (where $n = n_1 + n_2$ is the total particle density and σ the particle diameter), its concentration is put equal to zero. In this limit, $n_1 = n$ and $K^{\mathrm{MC}}(q;t)$ takes on the form known from one-component systems [7].

The long-time limit of the normalized relaxation function $\phi(q;t) := \Phi(q;t)/\Phi(q;t=0)$, usually denoted by $f(q)$ and referred to as the Debye-Waller factor, characterizes the arrest of density fluctuations and can thus be used to determine whether the system is a glass $[f(q)\neq 0]$ or a fluid $[f(q)\equiv 0]$. Making use of $\phi(q;t=\infty) = -\lim_{z\to i0} z\phi(q,z)$, the Debye-Waller factor can be obtained from Eq. (2) in the limit $z\to i0$,

$$f(q)=\frac{1}{1+\Omega^2(q)/K^{\mathrm{MC}}(q;t=\infty)}. \tag{12}$$

Note that $K^{\mathrm{MC}}(q;t=\infty)$ still contains $f(q)$ according to Eq. (10), so that Eq. (12) has to be solved iteratively for $f(q)$.

III. PHASE DIAGRAM

Using the mean spherical approximation solution from Ref. [14] for the HSJ static structure factor $S(q)$, Eq. (12) was solved numerically on a 301-point wave number mesh for $f(q)$ at different thermodynamic parameters. The resulting fluid-glass phase diagram is shown in Fig. 1 as a plot of the critical packing fraction η_c as a function of the plasma parameter $\Gamma := 2\sqrt[3]{\eta}/T^*$ with the reduced temperature T^*

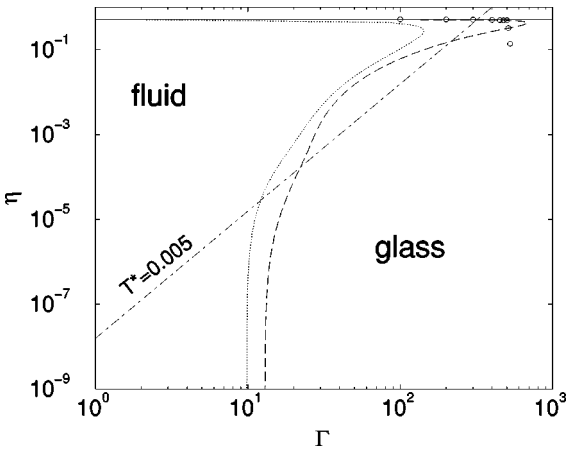

FIG. 1. Fluid-glass phase diagram for the HSJ (dashed), the RPM (dotted), and neutral hard spheres (solid). Ordinate: packing fraction η; abscissa: plasma parameter Γ. Circles are transition points taken from Ref. [16]. Dot-dashed: $\eta(\Gamma)$ at fixed temperature $T^*=0.005$.

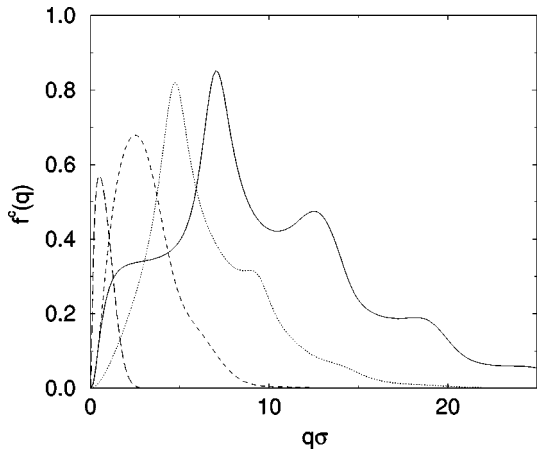

FIG. 2. Critical Debye-Waller factors $f^c(q)$ of the HSJ as a function of wave number q. Curves correspond to ($\eta\approx0.516$, $\Gamma\approx9.476$) (solid), ($\eta\approx0.120$, $\Gamma\approx167.6$) (dotted), ($\eta\approx0.005\,06$, $\Gamma\approx36.33$) (dashed), and ($\eta\approx0.39\times10^{-5}$, $\Gamma\approx15.74$) (long-dashed).

$:=k_BT4\pi\epsilon_0\sigma/(\mathrm{Ze})^2$. Ze is the charge of the hard spheres.

First, note that in the weak-coupling limit $\Gamma\to0$, the critical packing fraction approaches 0.516, the value known from neutral hard-sphere systems [15]. This was expected because the $S(q)$ used in the present calculation is known to approach the Percus-Yevick neutral hard-sphere structure factor in the weak coupling limit. Physically, the reason is that the Coulomb energy can be neglected compared to the thermal energy in this limit, leaving an effectively uncharged system.

In the high-density regime, our calculation reproduces the transition points recently found by Lai and Chang [16], except for one data point. The HSJ shows a reentrant phenomenon in the temperature interval $0.002<T^*<0.01$: Upon isothermally expanding the high-density glass along the dot-dashed line in Fig. 1, the system first melts, but then temporarily re-enters a glass phase before finally melting again to stay in the fluid phase for all lower densities. Similar reentrant phenomena have been found in mode-coupling studies of the RPM [9], of *screened* charged hard spheres [17] provided that the screening length was chosen sufficiently large, and in a theoretical investigation of macroionic suspensions [18]. In the low-density part of the reentrant region, $10^{-3}<\eta<5\times10^{-5}$, the HSJ glass transition curve exhibits a power law $\eta\propto\Gamma^{\alpha}$ with an exponent $\alpha\approx8.14$. So far, neither this behavior nor the reentrant phenomenon could be explained theoretically.

Even for very low densities, $\eta<10^{-6}$, mode-coupling effects obviously still lead to a structural arrest of the fluid of charged particles if temperature is sufficiently low. This is rather surprising, because the static structure factor does not exhibit any peaks in this limit—in *high-density* liquids, the first peak in $S(q)$, reflecting a close packing of the system, was considered to be the driving factor for the glass transition [7,19].

The melting curve of the HSJ takes on the form $\Gamma=\mathrm{const}$, or $\eta_c\propto(T_c^*)^3$, for $\eta<10^{-7}$. This result can be understood from the fact that the static structure takes on Debye form,

$$S_D(q)=\frac{q^2}{q^2+q_D^2},\quad c_D(q)=-\frac{1}{n}\frac{q_D^2}{q^2},\tag{13}$$

in the low-density limit, where $q_D^2:=n(\mathrm{Ze})^2/(\epsilon_0k_BT)=24\eta/(T^*\sigma^2)$, i.e., $1/q_D$ is the Debye-Hückel screening length. Inserting Eq. (13) into the MCT expression for the Debye-Waller factor, Eq. (12), one obtains

$$\frac{f(q)}{1-f(q)}=\frac{q_D^4}{n(q^2+q_D^2)V}\times\sum_{\mathbf{k}}\frac{(k_\parallel p^2+p_\parallel k^2)^2}{k^2(k^2+q_D^2)p^2(p^2+q_D^2)}f(k)f(p),\tag{14}$$

with $\mathbf{p}:=\mathbf{q}-\mathbf{k}$. Rescaling the wave numbers by q_D, the dependence on η and T^* reduces to the wave number scale and to a single coupling parameter $q_D^3/n\propto\Gamma^{3/2}$ in front of the integral. Thus, a glass transition must occur at some fixed Γ_c in the Debye region of the phase diagram. We find $\Gamma_c\approx13.0$ for the critical plasma parameter of the HSJ.

The phase diagram of the RPM from Ref. [9] is also included to demonstrate that the qualitative form, and in particular the ability to form a Wigner glass, do not depend on the specific model system. This supports our view that the reentrant phenomenon and the Wigner glass found in the RPM are not artifacts of a model system but general features of Coulomb systems caused by mode-coupling effects.

IV. DEBYE-WALLER FACTOR

Some of the Debye-Waller factors that were calculated along the phase transition line of Fig. 1 are shown in Fig. 2. The corresponding input information, the structure factor $S(q)$, is plotted in Fig. 3. For the high-density glass phase, $f(q)$ has the form known from previous calculations [16], especially the dominant peak at $q\approx7\sigma^{-1}$ reflecting the corresponding close-packing peak in the structure factor $S(q)$. As the critical density is decreased, this peak shifts to lower

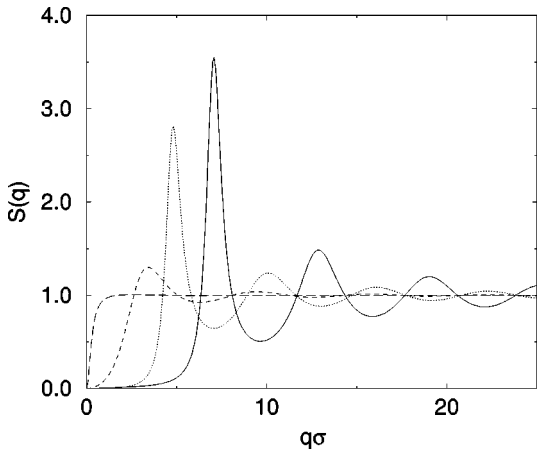

FIG. 3. Structure factor $S(q)$ of the HSJ for the same η and Γ as in Fig. 2.

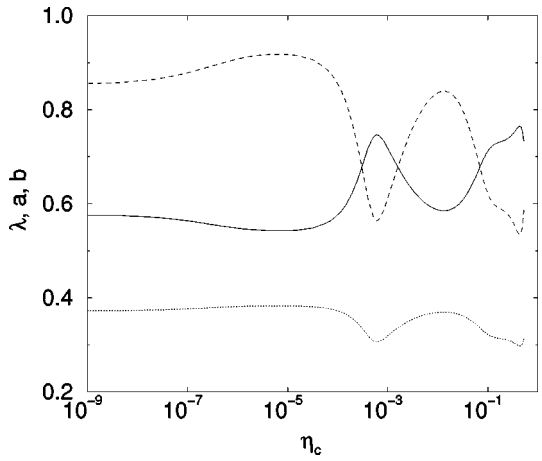

FIG. 4. HSJ exponent parameter λ (solid) and characteristic exponents a (dotted line) and b (dashed) as functions of the critical packing fraction η_c.

wave numbers and its height decreases. This is also the case for the $S(q)$ peak, signaling the decay of the close-packed structure of the high-density glass.

At very low densities, where the static structure takes on Debye form, Eq. (13), $f(q)$ becomes extremely narrow. This can be understood directly from rescaling Eq. (14) as explained in connection with the T^3 behavior of the transition line. It is found that in the Debye limit, the critical Debye-Waller factor can be written as $f_D(q/q_D)$, where f_D is a fixed master function, while the relevant wave number scale q_D vanishes like $\eta^{1/3}$ for $\eta \to 0$ on the transition line. In contrast to the static structure, which exhibits no peaks at all, there remains a peak in the Debye-Waller factor at $q \approx q_D$.

The property $f(q=0)=0$, which is clearly visible in Fig. 2, is due to momentum conservation. This can be seen as follows: Overall momentum conservation requires the determinant of the matrix $\hat{K}^{MC}(q;t=\infty)$ to vanish like q^2 for small wave numbers, a condition that is obeyed by the mode-coupling approximation [13]. It is clear from the derivation of Sec. II, however, that the background species does not carry any momentum. This leaves the momentum conservation condition for the matrix element for species 1 only,

$$K^{MC}(q;t=\infty) \propto q^2 \quad \text{for} \quad q \to 0. \tag{15}$$

The fact that $\Omega^2(q)$ approaches the (non-vanishing) plasma frequency $\omega_{pl}^2=(Ze)^2 n/(\epsilon_0 m_1)$ in this limit thus leads to $f(q=0)=0$ via Eq. (12). This property, which results from the idealization of a homogeneous background, has an important consequence for the HSJ as a model system. Since the mass- and charge-density relaxation functions $\phi_M(q;t)$ and $\phi_C(q;t)$ are identical to $\phi(q;t)$ in this system, $f(q=0)=0$ implies $\phi_C(q=0;\ t=\infty)=0$. This means that long-wavelength plasma oscillations cannot be arrested and the dielectric constant $\epsilon=1/\phi_C(q=0;\ t=\infty)$ of the HSJ will be infinite always, even in the glass phase. The same statement holds for the OCP.

From the Debye-Waller factors calculated at the transition point, the Götze exponent parameter λ can be obtained [20]. It characterizes the dynamical behavior predicted by MCT near the glass transition. To calculate the exponent parameter, the (nondegenerate, properly normalized) right and left eigenvectors $e(q)$ and $\hat{e}(q)$, respectively, of the stability matrix

$$C(q,k) := [1-f(k)]^2 \Sigma_{\mathbf{p}} 2\beta^2 S(k)S(p)V(\mathbf{q};\mathbf{k};\mathbf{p})f(p)/\Omega^2(q)$$

have to be determined at a transition point using an appropriate wave vector mesh. The exponent parameter of the transition point is then obtained from

$$\lambda := \sum_{\mathbf{qkp}} \hat{e}(q)\beta^2 S(k)S(p)\Omega^{-2}(q)V(\mathbf{q};\mathbf{k};\mathbf{p}) \times [1-f(k)]^2[1-f(p)]^2 e(k)e(p), \tag{16}$$

and the exponents a and b of the power laws that appear in the solution of Eq. (2) are determined by the equation $\Gamma(1-x)^2/\Gamma(1-2x)=\lambda$, which has the solutions $x=a$ and $x=-b$. Figure 4 shows a plot of the values of λ, together with the corresponding exponents a and b, along the transition line. For high temperatures, the exponent parameter approaches the limiting value 0.734, which is in agreement (relative deviation ≈3%) with the value 0.758 found for neutral hard spheres [15]. As conjectured by Götze [19], λ varies only between 0.5 and 1 in the whole density range studied. At small densities $\eta < 10^{-4}$, λ takes on extraordinarily small values ($\lambda < 0.6$), which leads to almost exponential relaxation behavior to be discussed in the next section.

V. RELAXATION BEHAVIOR

Using the same static structure as in Sec. IV, Eqs. (2) and (5) were solved iteratively for 540 time mesh points and 151 wave numbers. The regular part of the relaxation kernel, which determines the short-time dynamics and the overall time scale of the solutions only, was assumed to be diagonal with $\hat{K}_{11}^{reg}(q;t)=2\delta(t)\omega_{pl}(q\sigma)^2$. This order of magnitude was found in previous studies on the OCP [21].

A typical result for the (partial-) density relaxation function $\phi(q;t)$ for low densities is shown in Fig. 5 as a plot at a fixed wave number q_0 as the system approaches the fluid-glass transition at $\eta \approx 0.103 \times 10^{-4}$. The critical long-time

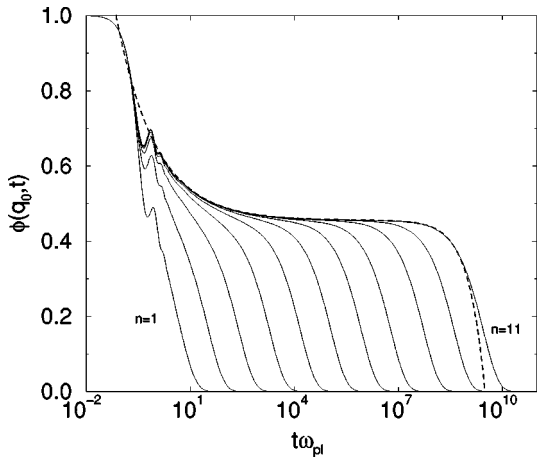

FIG. 5. Density relaxation function $\phi(q_0;t)$ of low-density HSJ at $q_0=\sigma^{-1}$. Curves correspond to $\eta\approx 0.103\times 10^{-4}$, $(T^*-T_c^*)/T_c^*=3^{-n}$ for $n=1,\ldots,11$, and $T_c^*\approx 0.002\,71$. Dotted: power law $0.455+0.2t^{-a}-9.1\times 10^{-10}t^b$ with $a=0.382$ and $b=0.916$.

limit $f^c(q_0)\approx 0.455$ expected at the transition point is clearly visible as a plateau value. By analyzing the MCT equations analytically [20,19], one finds that $\phi(q_0;t)$ approaches $f^c(q_0)$ as a power law $\propto t^{-a}$. This initial relaxation process is referred to as β relaxation. At a strongly temperature-dependent time τ_α, $\phi(q_0;t)$ drops down from the plateau with another power law $\propto -t^b$, and approaches zero. The latter process is the so-called α relaxation or primary relaxation. The α-relaxation time scale τ_α is predicted to obey the power law $\tau_\alpha\propto(T-T_c)^{-\gamma}$ with the exponent $\gamma:=1/(2a)+1/(2b)$. To demonstrate that these predictions hold for the numerically calculated function, the two asymptotic power laws are also included in Fig. 5, and the transition point was approached using temperatures T_n^* with $(T_c^*-T_n^*)/T_c^*=3^{-n}$, $n=1,2,3,\ldots$. This leads to an α-relaxation time that increases by constant factors.

If properly rescaled, the relaxation function of the supercooled low-density fluid looks qualitatively similar to the relaxation functions known from systems near the high-density glass transition. As mentioned in Sec. IV, the relevant length scale gets larger and larger at low densities. Therefore, $\phi(q;t)$ (considered as a function of q) becomes increasingly narrow in the low-η region. It is remarkable, however, to see that in the low-density Coulomb fluid we find oscillations of $\phi(q;t)$ with time t which are reminiscent of the (long-wavelength) plasma oscillation. Such oscillations are characteristic of the long-range Coulomb potential. They have neither appeared in supercooled binary mixtures of neutral particles (cf. Fig. 6 of Ref. [22]) nor in the high-density region (where Coulomb interactions are suppressed) of the present system (cf. Fig. 7.1 of Ref. [23]).

The small value $\lambda=0.543$ predicted for the transition at $\eta=0.103\times 10^{-4}$ leads to $a=0.382$ and $b=0.916$. The exponent b that rules the primary relaxation is therefore significantly larger than known from high-density systems, where $\lambda\approx 0.750$ implies $b\approx 0.558$. This results in a comparably abrupt drop from the plateau value at the beginning of the α-relaxation process and a relaxation that is much closer to the simple exponential Debye relaxation than the stretched α relaxation known from supercooled high-density liquids. The small values of the exponent parameter λ shown in Fig. 4 for low η imply that the primary relaxation is almost Debye-like for all densities $\eta<10^{-4}$.

Apart from the peculiarity of almost-exponential relaxation, all predictions that were derived for the liquid-glass transition at higher densities [20,19], e.g., the factorization of time- and wave number dependence in $\phi(q_0;t)-f^c(q_0)$ for long times, continue to be valid at low densities. It must be mentioned that the extremely small values $\lambda<0.6$ at low densities are a special feature of the HSJ, and were not found in the RPM, where $\lambda=0.77$ in the low-density limit [10]. Therefore, the exponential relaxation should not be considered as an universal prediction of MCT for Wigner glasses, but rather as a special feature of the HSJ model system. Nevertheless, it is an interesting question whether it is found experimentally, because this would allow an estimation of the relevance of the MCT/HSJ model system for Wigner glass experiments.

VI. TRANSPORT PROPERTIES

A. Diffusion

The mobility of individual particles within the fluid is described by the diffusion constant D. This parameter should be easily accessible in Wigner glass experiments, because it can be measured directly from the observation of particles in the fluid. Theoretically, D is determined by the incoherent relaxation function $\Phi_s(q;t):=\beta\langle\exp\{i\mathbf{q}\cdot[\mathbf{r}_0^{(1)}(t)-\mathbf{r}_0^{(1)}(t=0)]\}\rangle$ for $q\neq 0$, which can be obtained within MCT by solving the set of equations [7]

$$\Phi_s(q,z)=\frac{-\beta}{z+q^2v_{th}^2/z+K_s(q,z)}, \tag{17}$$

$$K_s(q,z)=K_s^{reg}(q,z)+K_s^{MC}(q,z), \tag{18}$$

$$K_s^{MC}(q;t)=\frac{v_{th}^2 n}{\beta^2}\frac{1}{V}\sum_{\mathbf{k}} k_\parallel^2 c(k)^2\Phi(k;t)\Phi_s(|\mathbf{q}-\mathbf{k}|;t), \tag{19}$$

where $v_{th}^2:=1/(\beta m_1)$ denotes the thermal particle velocity. Note that the coherent relaxation function $\Phi(q;t)$ must be known before $\Phi_s(q;t)$ can be determined. The frequency-dependent generalized diffusion constant $D(\omega)$ is given by

$$D(\omega)=\lim_{q\to 0}\mathrm{Im}\left\{\frac{-v_{th}^2}{\omega+K_s(q,\omega+i0)}\right\}. \tag{20}$$

Assuming $K_s^{reg}(q;t)=20\omega_{pl}\delta(t)$, Equations (17)–(19) were solved iteratively. The resulting diffusion constant is plotted in Fig. 6. The most striking feature is the rapid decrease of the static value $D=D(\omega=0)$ as the glass transition is approached. MCT predicts a vanishing of D with a power law $(T-T_c)^\gamma$ near the glass transition, where γ is the exponent defined in section V [20]. This behavior is clearly visible in the inset of Fig. 6. Physically, the vanishing of D upon approaching the low-density glass transition can be understood by considering that diffusion is blocked by rapidly increasing

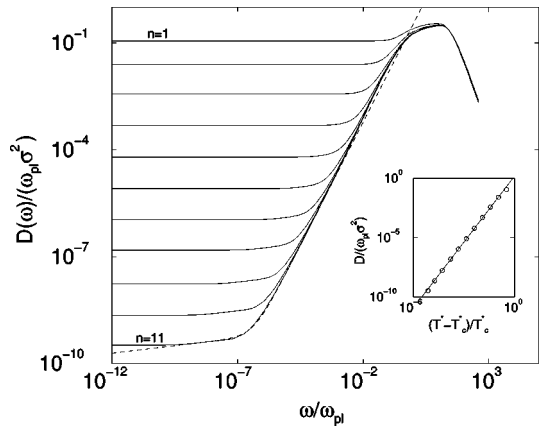

FIG. 6. Generalized diffusion constant $D(\omega)$ of the HSJ for the same parameters (η,T^*) as in Fig. 5. Dashed: MCT power law asymptote $2.0\times10^{-9}\omega^{1-b}+0.35\omega^{1+a}$ with a and b as in Fig. 5. Inset: D as a function of $(T^*-T_c^*)/T_c^*$ (circles). Solid: power law $1.5[(T^*-T_c^*)/T_c^*]^{\gamma}$ with $\gamma:=1/(2a)+1/(2b)=1.852$.

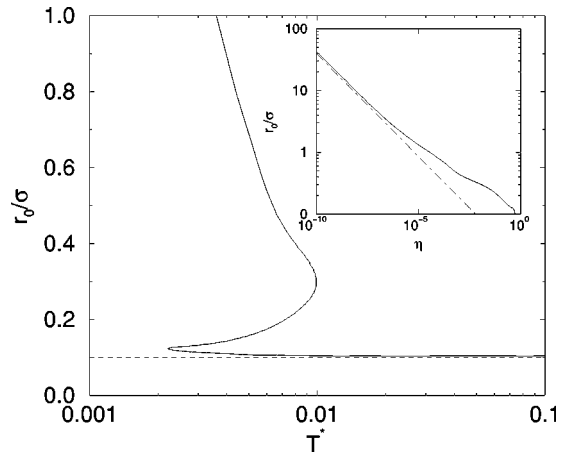

FIG. 7. HSJ localization length at melting as function of temperature T^* (solid) and Lindemann criterion $r_0=0.1\sigma$ (dashed). Inset: Same data as a function of η (solid), and power law $0.02\eta^{-1/3}$ (dot-dashed).

effective particle diameters. Neglecting screening effects, the average thermal energy at $\Gamma=10$ and $\eta=10^{-6}$, e.g., allows two particles to approach each other no closer than about 500 times the particle diameter! Even if the system *looks* very dilute, it is a strongly overlapping packing of soft effective Coulomb spheres. The slowing down of diffusion processes due to this effect will eventually prohibit crystallization of the low-density fluid experimentally if it is cooled rapidly enough, and is therefore responsible for the glass transition at low densities.

The two power laws that rule the frequency dependence of $D(\omega)$ can be explained by considering the asymptotic solution for $\Phi_s(q;t)$ at the transition point [20]. One finds $D(\omega)\propto\omega^{1-b}$ in the α-relaxation region, and $D(\omega)\propto\omega^{1+a}$ in the frequency range corresponding to β relaxation, which is clearly reproduced by our numerical calculations. If these power laws are identified in experimental data, the values for the exponents a and b could be used to determine the exponent parameter λ experimentally.

B. Localization length

On the glassy side of the transition, the particles are localized, so that $D=0$. Here, the motion of a single tagged particle can be characterized by its localization length r_0,

$$r_0^2:=\tfrac{1}{3}\lim_{t\to\infty}\langle[\mathbf{r}_0^{(1)}(t=0)-\mathbf{r}_0^{(1)}(t)]^2\rangle=-\lim_{q\to0}\frac{\partial^2 f_s(q)}{\partial q^2}, \tag{21}$$

where $f_s(q):=\lim_{t\to\infty}\Phi_s(q;t)/\beta$ denotes the long-time limit of the tagged particle relaxation function, the Lamb-Mößbauer factor. Despite of its complicated calculation, the function $f_s(q)$ turns out to be very similar to a simple Gaussian, $f_s(q)\approx\exp(-\frac{1}{2}r_0^2q^2)$. This well-known fact for the high-density glass [7] continues to be valid even at very low densities.

The localization length r_0 at melting obtained from the Lamb-Mößbauer factor is plotted in Fig. 7 along the transition line. An empirical rule for the relation between melting of a solid and the localization length is the Lindemann criterion [24], which predicts melting if r_0 exceeds 10% of the particle diameter. As found in previous studies on different model systems [7,25], the high-density glass transition predicted by MCT is in agreement with this criterion. At low densities, however, the localization length of particles in the Wigner solid can be much greater than predicted by the Lindemann criterion. Our calculations predict a critical r_0 of about 2.3σ at $\eta=10^{-6}$, for example. Such large values for r_0 have also been observed experimentally, e.g., in the video images shown in Ref. [26]. These results indicate that the particles of a Wigner solid are trapped in extremely flat, extended potential minima.

Similarly to the Debye-Waller factors, the Lamb-Mößbauer factors $f_s(q)$ will also fall onto a single master function if rescaled by the Debye shielding length q_D^{-1}. Thus, their curvature at $q=0$, which is proportional to r_0, should diverge as $1/q_D\propto1/\sqrt[3]{\eta}$ along the transition line, where $\eta\to0$ and $T^*\propto\eta^{1/3}$. The inset of Fig. 7 demonstrates that this property is correctly reproduced by our numerical results.

C. Shear viscosity

The most striking signature of the high-density glass transition is the dramatic increase of the shear viscosity η_s of the fluid. Therefore, it is an important question whether this increase is also predicted for the supercooled fluid at low densities as the Wigner glass phase is approached. Within MCT, η_s can be calculated without any further approximations from the transversal current relaxation kernel [19]

$$K_\perp^{MC}(q;t)=\sum_{\mathbf{kp}}V_\perp(\mathbf{q};\mathbf{k};\mathbf{p})\Phi(k;t)\Phi(p;t), \tag{22}$$

$$V_\perp(\mathbf{q};\mathbf{k};\mathbf{p}):=\frac{n}{\beta^3 m_1}\frac{1}{V}\delta_{\mathbf{p},\mathbf{q}-\mathbf{k}}k_\perp^2[c(k)^2-c(k)c(p)], \tag{23}$$

which can be obtained from the relaxation function $\Phi(q;t)$. The frequency-dependent generalization η_s of the shear viscosity is then given by

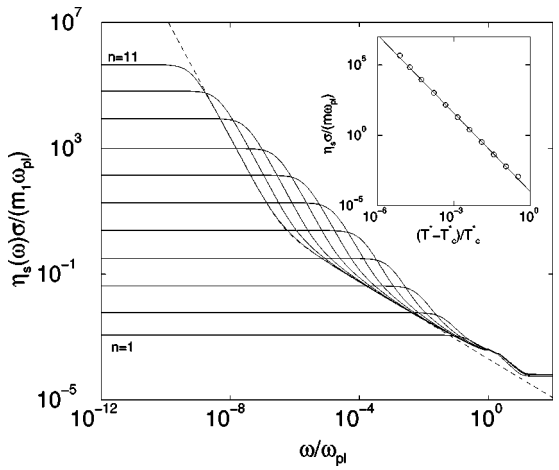

FIG. 8. Generalized shear viscosity $\eta_s(\omega)$ of the HSJ for the same parameters (η,T^*) as in Fig. 5. Dashed: MCT power law asymptote $1.0\times10^{-12}\omega^{-b-1}+2.0\times10^{-4}\omega^{a-1}$ with a and b as in Fig. 5. Inset: η_s as a function of $(T^*-T_c^*)/T_c^*$ (circles). Solid: power law $10^{-4}[(T^*-T_c^*)/T_c^*]^{-\gamma}$ with γ as in Fig. 5.

$$\eta_s(\omega)=m_1 n\lim_{q\to0}\frac{\mathrm{Im}\,K_\perp(q,\omega+\mathrm{i}0)}{q^2}. \tag{24}$$

Note that in the units we use, the shear viscosity η_s is related to the kinematic viscosity $\nu:=\eta_s/(nm_1)$ by

$$\frac{\nu}{[\sigma^2\omega_{pl}]}=\frac{\pi}{6\eta}\frac{\eta_s}{[m_1\omega_{pl}/\sigma]}. \tag{25}$$

The shear viscosity $\eta_s(\omega)$ was calculated from the relaxation functions of Fig. 5 under the assumption that the regular part of the transversal current relaxation kernel is $K_\perp^{\mathrm{reg}}(q;t)=2\omega_{pl}\delta(t)$. The resulting functions, which are plotted in Fig. 8, look qualitatively like the viscosities known from the high-density liquid-glass transition. MCT predicts a divergence of the η_s proportional to $(T-T_c)^{-\gamma}$ as the transition is approached. This property is demonstrated in the inset of Fig. 8. Note that γ is the same exponent that governed the behavior of the diffusion constant D [20]. Similarly to the behavior of $D(\omega)$, $\eta_s(\omega)$ also exhibits power laws in the frequency ranges of α and β relaxation. The corresponding exponents can be shown to be $-b-1$ and $a-1$, respectively. The viscosity of the low-density fluid turns out to be several orders of magnitude smaller than that of a high-density liquid at a comparable separation from the transition point.

It seems counterintuitive to obtain an infinite shear viscosity for a Wigner glass, which one imagines to be a loose matrix of relatively ''soft'' spheres. However, it is generally accepted for the high-density liquid-glass transition that the divergence of the shear viscosity is an artifact of idealized MCT. The results of this version of the theory are only valid in a region of low to intermediate viscosity, which we expect to be the case for the Wigner glass as well. The actual range of validity of idealized MCT for supercooled low-density fluids can only be determined experimentally—a challenge for plasma and colloid physicists.

Having calculated the diffusion constant and the shear viscosity, we will now make use of the Stokes-Einstein relation

$$D=\frac{k_B T}{4\pi\eta_s R}, \tag{26}$$

known from liquid physics to obtain the Stokes radius $R=R(\eta,T^*)$ measuring the effective particle size. The Coulomb fluid near the glass transition does not obey the kinetic theory of gases even at low densities, because the long-range interactions remain strong and cannot be neglected in comparison to the kinetic energy of particles. Therefore, it is reasonable to assume for the supercooled fluid a relation between D and η_s of the Stokes-Einstein form even at low densities. We calculated R in the vicinity of three different glass-transition points in the (η,T^*) plane and obtained $R/(\sigma/2)\approx0.8$, 1×10^4, and 2×10^5 at high ($\eta\approx0.51$), intermediate ($\eta\approx0.10\times10^{-4}$), and low ($\eta\approx0.86\times10^{-8}$) density, respectively.

At high densities and correspondingly high temperatures, the Coulomb interaction is strongly suppressed, and we find that the Stokes radius is roughly equal to the hard-core radius. This means that MCT predicts validity of the Stokes-Einstein relation for the HSJ at high densities, a result that is supported by a molecular dynamics simulation of uncharged soft spheres [27] also reporting that the relation is well fulfilled in the supercooled region.

The long-range Coulomb force will become effective if temperature is decreased. It will be the dominant interaction near the low-density glass transition. At low densities according to our results above, the Stokes radius R takes on values much larger than the hard-core radius $\sigma/2$ and even larger than the average available-sphere radius $(4\pi n/3)^{-1/3}$. This can be understood by the following argument. The big Coulomb particles discussed in Sec. VI A will, due to the long range of interactions, have an overlap with very many neighboring fluid particles. The diffusion constant D for such an inflated particle is expected to be small even if the viscosity η_s of the fluid is still relatively low. According to Eq. (26), this implies a large Stokes radius R.

VII. CONCLUSION

In view of experiments, it is important to judge the relevance of the results of our study carefully. First of all, neither quantum nor relativistic effects are relevant in the low-density region of the phase diagram. A major point of criticism may be that the *idealized* form of MCT was used, which is known to neglect hopping diffusion and to yield a sharp transition into a nonergodic glass phase. We argue, however, that the obtained results are still relevant. Hopping diffusion processes occurred only ''occasionally'' in the Wigner crystal [5]. Assuming an average hopping time of $\tau_H=10^4$ s for an individual particle and a microscopic time scale of $t_0\approx10^{-4}$ s, suggests that there are several decades of time evolution in Fig. 5 which are not influenced by hopping diffusion. Taking hopping processes into account in an extended MCT [19] will change the relaxation behavior of the supercooled fluid only quantitatively without destroying qualitative aspects such as plateau formation and α and β

relaxation. Although the experimental relevance of the singularity that appears in idealized MCT is still being discussed controversially, the transition point of idealized MCT has always correctly signaled the onset of glassification in high-density systems. Thus, we expect the formation of a low-density glass in real systems in the proximity of our calculated transition curve.

On the other hand, we cannot derive any statements on the actual range of validity of the power law predictions. Theoretically, they become valid *asymptotically*, i.e., for ''small'' separation from the transition point—possibly in a region where idealized MCT is no longer experimentally relevant. This point should always be kept in mind when interpreting experimental results using MCT. However, experience from high-density liquids tells us that some asymptotic MCT predictions, depending on the system studied, seem to have been observed in experiments [28].

In summary, we have found that mode-coupling theory predicts a low-density amorphous solid phase of the HSJ. The transition is expected to occur at $\Gamma \approx 13$ in the low-density region $\eta < 10^{-7}$. The HSJ exhibits the reentrant phenomenon found in mode-coupling studies of the RPM [9] and of screened charged hard spheres [17]. The relaxation is qualitatively similar to that predicted for the higher-density liquid-glass transition, except for an almost exponential α relaxation. We proposed the picture of a packing of large effective spheres caused by Coulomb repulsion in the Wigner glass, which is supported by a vanishing of the diffusion constant as the glass transition is approached and by a very large Stokes radius.

It is very exciting that Wigner crystals were found in dusty plasmas, where individual particles can be studied using optical microscopes. The realization of Wigner *glasses* in such systems would be a major breakthrough in the research on the glass transition, because one could ''see'' how the individual particles become localized within the glassy matrix. Until today, rather complicated and expensive scattering experiments are the only source of microscopic information on the glass transition.

ACKNOWLEDGMENT

This work was supported by the Deutsche Forschungsgemeinschaft (SFB 337).

[1] E. Wigner, Trans. Faraday Soc. **34**, 678 (1938).
[2] H. W. Jiang, R. L. Willett, H. L. Stormer, D. C. Tsui, L. N. Pfeiffer, and K. W. West, Phys. Rev. Lett. **65**, 633 (1990).
[3] D. H. Van Winkle and C. A. Murray, J. Chem. Phys. **89**, 3885 (1988).
[4] J. H. Chu and I. Lin, Phys. Rev. Lett. **72**, 4009 (1994).
[5] H. Thomas, G. E. Morfill, V. Demmel, J. Goree, B. Feuerbacher, and D. Möhlmann, Phys. Rev. Lett. **73**, 652 (1994).
[6] H. Aoki, J. Phys. C **12**, 633 (1979).
[7] U. Bengtzelius, W. Götze, and A. Sjölander, J. Phys. C **17**, 5915 (1984).
[8] E. Leutheusser, Phys. Rev. A **29**, 2765 (1984).
[9] J. Bosse and S. D. Wilke, Phys. Rev. Lett. **80**, 1260 (1998).
[10] H.-C. Chen, S. D. Wilke, and J. Bosse (unpublished).
[11] H. Mori, Prog. Theor. Phys. **33**, 423 (1965); **34**, 399 (1965).
[12] R. Zwanzig, in *Lectures in Theoretical Physics*, edited by W. Brittin and L. Dunham (Wiley-Interscience, New York, 1961), Vol. 3, p. 135ff.
[13] J. Bosse, Z. Phys. B **103**, 357 (1997).
[14] R. G. Palmer and J. D. Weeks, J. Phys. (France) **58**, 4171 (1972).
[15] J. L. Barrat, W. Götze, and A. Latz, J. Phys.: Condens. Matter **1**, 7163 (1989).
[16] S. K. Lai and S. Y. Chang, Phys. Rev. B **51**, 12 869 (1995).
[17] S. K. Lai, W. J. Ma, W. van Megen, and I. K. Snook, Phys. Rev. E **56**, 766 (1997).
[18] S. Khan, T. L. Morton, and D. Ronis, Phys. Rev. A **35**, 4295 (1987).
[19] W. Götze, in *Liquids, Freezing, and the Glass Transition*, edited by D. Levesque, J. P. Hansen, and J. Zinn-Justin (North-Holland, Amsterdam, 1991), Vol. I, p. 289.
[20] W. Götze, Z. Phys. B **60**, 195 (1985).
[21] J. Bosse and T. Munakata, Phys. Rev. A **18**, 2337 (1978).
[22] J. Bosse, M. Groß, and Y. Kaneko, in *Quasielastic Neutron Scattering*, edited by J. Colmenero, A. Alegría, and F. J. Bermejo (World Scientific, Singapore, 1994), p. 38.
[23] S. D. Wilke, Diploma thesis, Freie Universität Berlin, 1998.
[24] F. A. Lindemann, Phys. Z. **11**, 609 (1910).
[25] U. Bengtzelius, Phys. Rev. A **33**, 3433 (1986).
[26] M. H. Thomas and G. E. Morfill, Nature (London) **379**, 806 (1996).
[27] J. L. Barrat, R. N. Roux, and J.-P. Hansen, Chem. Phys. **149**, 197 (1990).
[28] H. Z. Cummins, G. Li, Y. H. Hwang, G. Q. Shen, W. M. Du, J. Hernandez, and N. J. Tao, Z. Phys. B **103**, 501 (1997).